

Emergent Hydrodynamic Bound States Between Magnetically Powered Micropropellers

Fernando Martinez-Pedrero,^{1,2} Eloy Navarro-Argemí,¹
Antonio Ortiz-Ambriz,¹ Ignacio Pagonabarraga,^{1,3}, Pietro Tierno^{1,3,4*}

¹Departament de Física de la Matèria Condensada, Universitat de Barcelona, Barcelona, Spain

²Departamento de Química Física I, Universidad Complutense de Madrid, Madrid, Spain

³Universitat de Barcelona Institute of Complex Systems (UBICS), Barcelona, Spain

⁴Institut de Nanociència i Nanotecnologia, IN²UB, Universitat de Barcelona, Barcelona, Spain

*To whom correspondence should be addressed; E-mail: ptierno@ub.edu.

Hydrodynamic interactions (HIs), namely solvent mediated long-range interactions between dispersed particles, play a crucial role in the assembly and dynamics of many active systems, from swimming bacteria to swarms of propelling microrobots. Here we experimentally demonstrate the emergence of long-living hydrodynamic bound states between model micro-swimmers at low Reynolds number. A rotating magnetic field forces colloidal hematite microparticles to translate at a constant and frequency-tunable speed close to a bounding plane in a viscous fluid. At high driving frequency, HIs dominate over magnetic dipolar ones, and close propelling particles couple into bound states by adjusting their translational speed in order to optimize the transport of the pair. The physical system is described by considering the HIs with the boundary surface and the effect of gravity, providing an excellent agreement with the experimental data for all the range of parameters explored. Moreover, we

show that in dense suspensions, these bound states can be extended to one-dimensional arrays of particles assembled by the sole HIs. Our results manifest the importance of the boundary surface in the interaction and dynamics of confined propelling microswimmers.

INTRODUCTION

Active particles moving in viscous fluids driven by external fields (1–5) or chemical reactions (6, 7), represent a rich and growing area of research where many emergent non-equilibrium phenomena can be observed (8). The dynamics of an ensemble of active particles are governed by the interplay between propulsion, thermal noise and pair-interactions coupled with the dispersing medium. External fields usually induce alignment and fast assembly of the particles due to dipolar forces (9). Subtler is the role played by HIs, i.e. the solvent-mediated long-range interactions, that can be excited by the random or directed motion of the particles in the fluid medium. These interactions depend on the particle speed and angular velocities, since the solvent couples to the particles through forces and torques. Thus HIs cannot be described by a simple potential term, in contrast to dipolar forces.

Colloidal dispersions constitute a suitable model system to study the complex effects of HIs at low Reynolds number, given the ability to manipulate (10–13), align (14–16) or rotate (17–19) the particles with external fields. More generally, HIs are not only limited to colloids, but affect the dynamics of many complex and biological systems (20, 21). Examples span from the spontaneous formation of cell vortex arrays (22), to synchronized cilia beating (23, 24), and the attraction and dancing of a pair of algae *Volvox* (25). Thus, understanding the effect of HIs in interacting microscale objects is crucial in both applied and fundamental research.

When the motion of the propelled particles is affected by a nearby wall, the confinement may have a strong influence on the system dynamics. For example, the proximity of a surface

explains the circular path of motile *E. coli* (26), the attraction of model swimmers toward the surface (27), or can be even used to steer the particles along defined paths (28–31). Most of the experiments based on trapped or driven colloidal particles used as model system, have been mainly focused on the direct interactions between the couple, without exploring the effect of a confining plane on the collective dynamics.

Here we investigate the interactions between a pair of model microswimmers, composed of monodisperse ferromagnetic hematite microparticles driven above a plane by an external rotating magnetic field. At high driving frequencies, the spinning particles generate large hydrodynamic flow fields, and the corresponding HIs dominate over the magnetic ones, giving rise to different dynamic states. We report the direct experimental observation of hydrodynamic bound states with a long lifetime, where two close propelling particles adjust their velocities in order to couple their trajectory. Depending on the relative position of the particles, the bound colloids could either translate tip to tip, or speed up by aligning such that the relative position is perpendicular to the particles' long axes. The experiments are complemented with a theoretical model that takes into account the presence of the bounding plane, allowing to capture the essential physics of the process.

RESULTS

In our experiments, we use "peanut" shaped hematite microparticles, characterized by a long (short) axis equal to $a = 2.5\mu\text{m}$ ($b = 1.4\mu\text{m}$), Figs.1(a,b). After dilution in highly deionized water, the particles sediment due to density mismatch above a glass substrate, where they display small Brownian motion with negligible out-of plane fluctuations. The particles have a small permanent moment m perpendicular to their long axis. We determine the amplitude of the particle moment by following the orientational angle θ of individual particles when subjected to a static magnetic field H . Fig.1(c) shows the evolution with time of θ for 5 different parti-

cles and the corresponding fits to the experimental data, see the Method section. From these fits, we find a distribution of moments $P(m)$ centered at $\langle m \rangle = 9 \cdot 10^{-16} \text{A m}^2$, and having a Gaussian-like shape with variance $\sigma_m = 3 \cdot 10^{-16} \text{A m}^2$.

We spin the hematite particles by applying a rotating magnetic field circularly polarized in the (\hat{x}, \hat{z}) plane, $\mathbf{H}(t) = H_0(\cos(\omega t)\mathbf{e}_x - \sin(\omega t)\mathbf{e}_z)$ with angular frequency ω and amplitude H_0 , Fig.1(a). The applied modulation induces a magnetic torque $\mathbf{T}_m = \mu_0 \mathbf{m} \times \mathbf{H}$, which sets the particles in rotation close to the substrate at an average angular velocity $\langle \Omega \rangle$, with $\mu_0 = 4\pi \cdot 10^{-7} \text{H m}^{-1}$. The solid surface breaks the spatial symmetry, and the anisotropic particles roll close to the plane due to the rotation-translation hydrodynamic coupling (32). The net drift velocity is a function of the angular speed, $\langle v_x \rangle = b f_r \langle \Omega \rangle / 2$, being f_r a small correction factor resulting from the wall proximity. From the fit in Fig.1(d), and using the expression of f_r (33), we estimate the average elevation of the particle to be $h = 1.0 \mu\text{m}$. Below a critical frequency ω_c , single particles follow the field rotation synchronously, with $\langle \Omega \rangle = \omega$. For $\omega > \omega_c$ the particles follow asynchronously the driving magnetic field, and $\langle v_x \rangle$ decreases as the ω increases. Neglecting thermal fluctuations, the average rotational speed follows $\langle \Omega \rangle = \omega(1 - \sqrt{1 - (\omega_c/\omega)^2})$ (34), as shown by the blue fit in Fig.1(d). We note that the hematite particles display a weak magnetic-moment polydispersity, as also measured in Fig.1(c). As a consequence, close to ω_c , the propellers show a speed distribution, $P(\langle v_x \rangle)$, and similar particles may display different average speeds being in the synchronous or asynchronous regime.

When we increase the density of the colloidal system, close particles start to interact due to magnetic and viscous forces. The driving field aligns the permanent moments of the micro-propellers, ensuring that the particles always roll perpendicular to their long axis. Thus, only the angle ϑ between \hat{x} -axis and the line connecting the center of the two particles is needed to describe the relative orientation of the pair, Fig.1(e). In order to classify the type of dynamic

states observed, we vary mainly the driving frequency that controls the average speed, and fix the field amplitude. We find that the relative arrangements of pairs of particles strongly depend on their rotational motion. At low driving frequencies, $\omega \lesssim 125.7 \text{rads}^{-1}$, the propellers tend to arrange such that the relative position is perpendicular to the particles' long axes, in order to minimize the magnetic energy of the couple, first column of Fig.1(e). In contrast we find that, at high driving frequencies, the fast spinning of the particles induces strong HIs, and the propellers assemble forming a different bound state, in which the particles align along their long axis during propulsion, second column in Fig.1(e), even if dipolar interactions are repulsive in this configuration, as demonstrated in the next section.

We can identify the emergence of these bound states by measuring the order parameter $\alpha = (v_{rel}/v_{cv})^2$, based on the speed $v_{1,2}$ of the particles, which quantifies the ratio between the relative velocity $v_{rel} = v_1 - v_2$ and center of velocity $v_{cv} = (v_1 + v_2)/2$ of the couple. Figs.2(a-c) show three representative cases illustrating the behavior of a couple of propellers with the low frequency situation displayed in the first column. At high frequencies, we find that colloidal pairs tend to either align at a finite angle ($\vartheta \in [\pi/6, \pi/3]$), second column in Figs.2(a-c), or to arrange themselves parallel to each other such that $\vartheta = \pi/2$, third column in Figs.2(a-c). In the last two cases, the two particles form a transient hydrodynamic state that can last more than 6 seconds, and where the two particles adjust their velocities such that either v_{cv} increases ($\vartheta \rightarrow 0$) or decreases ($\vartheta \rightarrow \pi/2$), and v_{rel} almost vanishes. We quantify the duration of these bound states by measuring the histogram of the distribution of time lapses during which $\alpha < 0.01$. We find that with this choice, these states have a longer duration at high frequencies, even if magnetic interactions oppose their development, as shown by Figs.2(d,e). The presence of disorder and thermal noise in the experimental system may be at the origin of the finite lifetime of these states. However, we have found cases where the bound states were observed along the whole sample area, providing a strong indication that the observed trajectories do not

correspond to simple scattering events between the particles.

1 THEORETICAL MODEL

Hydrodynamic interactions. We model the propelling couple as a pair of rotating solid spheres above a wall. The solid surface can be accounted through an hydrodynamic singularity placed at the same distance below the position of the interface, namely a particle rotating in the opposite sense, plus additional stresslet and source doublets (35). We assume that the applied field forces the particles to rotate at a given angular velocity, which may differ from the driving frequency depending on the nature of each colloidal particle. Thus, the flow generated by a colloid of radius a and rotating at a prescribed angular velocity Ω , can be estimated by considering a rotlet located at a distance h from the wall:

$$\frac{u_i}{a^3} = \frac{\epsilon_{ijk}\Omega_j r_k}{r^3} - \frac{\epsilon_{ijk}\Omega_j R_k}{R^3} + 2h\epsilon_{kjl}\Omega_j \left(\frac{\delta_{ik}}{R^3} - \frac{3R_i R_k}{R^5} \right) + 6\epsilon_{kjl}\Omega_j \frac{R_i R_k R_l}{R^5}. \quad (1)$$

Here r is the position vector from the center of the particle and R the position of its image. From Eq.1 we derive analytic expressions for the speeds $v_{1,2}$ for two spheres 1, 2 rotating with angular speed $\Omega_{1,2}$ and at elevation $h_{1,2}$. The complete set of equations resulting from Eq.(1) are given in the Supplementary Information file.

From the model we can first resolve the complex dynamics of the particles in a bound state. Typical trajectories of the center of velocities of the two particles forming a pair are shown in Fig.3(a) and in MovieS4 in the Supplementary Information, when driven by an external rotating field in the synchronous regime. When the particles form the bound state, their relative distance is not fixed in one period, but the two propellers perform a periodic motion around each other in the 3D plane. During this motion, the particle elevation and their relative distance periodically vary thus, the type of bound orbit could depend on the initial angle and distance. This relative

motion can be clearly visualized from simulations, while being more difficult to be quantified from the experiments.

Role of gravity in the bound state We also consider the effect of gravity on the dynamics of the pair of particles. The gravitational force $F_g = \Delta\rho gV$ is balanced by the repulsive electrostatic interaction $F_{el} = \frac{A}{\lambda}e^{-z/\lambda}$ arising from the charge of the particle and the bounding plate. Here $V = (4/3)\pi a^3$ is the particle volume, $\Delta\rho$ is the density mismatch between the particle and the suspending medium, A a prefactor that depends on the surface charge density and λ the Debye screening length. For small displacement $z = h + \delta$, near the equilibrium elevation of the particle h , one can derive an effective elastic force with a coupling constant given by, $K = \frac{gV\Delta\rho}{\lambda}$. We consider the effect of the vertical forces as a stokeslet, and add its contribution to the Eq.1 in the Supplementary Information, where the resulting set of equation are given. These equations allow testing for the role of gravity in the bound state by varying the gravitational force $F_g = \Delta\rho gV$. In particular, in Fig.3(b) we plot the mean distance between two particles in a bound state as a function of the period of the rotating magnetic field. The different curves refer to situations where we vary the ratio $F_{g/h}$ between F_g and the viscous force $F_h = 3\pi\eta\Omega a^2/4$, being $\eta = 10^{-3}$ Pa · s the solvent viscosity and we used $h \sim a$ as the particle elevation from the substrate. In all cases we find that, for small initial distance between the particles, stable bound states with no particle separation can be formed in absence of gravity ($F_{g/h} = 0$) or even for strong gravitational forces ($F_{g/h} = 1$). Thus, we still observe the formation of these states and find that the main effect of gravity is to reduce the three-dimensional movement of the particles when they couple. The consequence of this constrained motion is that the relative positional angle between the particles changes, as shown in Fig.3(c). Starting from a configuration of $\vartheta = 45^\circ$, even small gravitational forces ($F_{g/h} \sim 10^{-2}$) are able to stabilize the couple of particle in the tip to tip configuration, illustrated in the second column of Fig.1(e). This configuration is linearly unstable for the purely hydrodynamic model, but it

becomes stable in presence of gravity.

Magnetic interactions. We here show that the dipolar interactions between a pair of propellers are effectively attractive (repulsive) when their relative position is perpendicular (parallel) to the particle long axis. The magnetic dipolar interactions between a pair of particles, (i, j) , with moments $\mathbf{m}_i, \mathbf{m}_j$ and at a distance $\mathbf{r}_{ij} = |\mathbf{r}_i - \mathbf{r}_j|$, is given by $U_d = \frac{\mu_0}{4\pi} \left(\frac{\mathbf{m}_i \mathbf{m}_j}{r_{ij}^3} - \frac{3(\mathbf{m}_i \cdot \mathbf{r}_{ij})(\mathbf{m}_j \cdot \mathbf{r}_{ij})}{r_{ij}^5} \right)$. Thus U_d is maximally attractive (repulsive) for particles with magnetic moments parallel (perpendicular) to \mathbf{r}_{ij} . If we consider two dipoles confined on the (x, y) plane, and aligned by a magnetic field rotating in a perpendicular plane (y, z) , as shown in Fig.1(a), we can calculate the average interaction energy between them by performing a time average (9). We find that the effective potential is attractive $\langle U_d \rangle = -\frac{\mu_0 m^2}{8\pi(x+z)^3}$, leading to chaining in the (\hat{x}, \hat{z}) plane, while being repulsive in the perpendicular plane (\hat{x}, \hat{y}) , $\langle U_d \rangle = \frac{\mu_0 m^2}{4\pi y^3}$.

Further, we can put forward a simple argument to explain the different arrangements from the changes in magnitude of the competing forces acting on the pair. The attractive force between two equal dipoles m at distance $r = 2a$ is given by $F_m = 3\mu_0 m^2 / (64\pi a^4)$, while the viscous force generated by a single propeller is $F_h = 3\pi\eta\Omega a^2 / 4$, being $\eta = 10^{-3} \text{Pa} \cdot \text{s}$ the solvent viscosity and $h \sim a$. Hence, for $m = 9 \cdot 10^{-16} \text{Am}^2$ and $a = b/2 = 0.7 \mu\text{m}$, we find that $F_h / F_m = 16\pi^2 \eta \Omega a^6 / (\mu_0 m^2) = 0.02\Omega$. Thus $F_h = 0.6F_m$ for $\Omega = 31.4 \text{rad s}^{-1}$, while $F_h = 9.1F_m$ for $\Omega = 504.6 \text{rad s}^{-1}$. Finally, we note that the magnetic interactions due to the permanent moments of the particles are relatively small, and the tip-to-tip (side-by-side) alignment gives an interaction potential $U_d = 7.3k_B T$ ($U_d = 1.3k_B T$), i.e. much lower than the interactions resulting from induced dipoles (36). Thus, while in our previous works (36, 37) the magnetic interactions were essential to maintain the propelling structures, here the dynamic states observed at large frequencies are bound purely by hydrodynamic interactions mediated through the confinement.

DISCUSSION

We test the model by measuring the average translational speed $\langle v_{cv} \rangle$ of a pair of particle in a bound state. In particular, we decompose this velocity in two components parallel ($\langle v_{cv} \rangle \cdot \hat{x}$) and perpendicular ($\langle v_{cv} \rangle \cdot \hat{y}$) to the propulsion direction (\hat{x} -axis) imposed by the rotating field. Both quantities, normalized with respect to the speed of a single propeller $\langle v_0 \rangle$, are plotted versus the positional angle ϑ in Figs.4(a,b), and at different center to center distances r . The image shows the comparison between the experimental data (symbols) and the analytical results (continuous line) which were plotted assuming that both particles have the same elevation, $h \sim 1\mu\text{m}$, as determined from the fits in Fig.1(d), and are driven in the synchronous regime with $\Omega_{1,2} = \omega = 502.6 \text{ rads}^{-1}$. The data and the fits show that along the propulsion direction, the pair of particles decreases their average speed with the angle ϑ , being the configuration where the relative position is perpendicular to the particles' long axes the fastest one. The behavior of the perpendicular component also illustrates the tendency of the pair to have a higher transversal velocity at intermediate angles, in agreement with the experimental observation where pair of propellers were found to speed up when placed at $\vartheta \sim 45^\circ$, see also Figs.2(b), second row. Despite the approximations in the model, we obtain quantitative agreement with the experimental data, as the model well captures the physical mechanism behind the HIs in these bound states.

Self-organization induced by HIs at low Reynolds number is of attracting remarkable interest due to its direct connection with assembly and swarming in active living systems (38–45). We demonstrate that our colloidal propellers, when driven at high frequencies, can be organized into metastable, elongated structures maintained only by HIs. Fig.5(a) shows a series of images illustrating the assembly process of a chain composed by 5 hydrodynamically coupled propellers driven by the rotating field. As shown in MovieS3 in the Supplementary Information, to assemble this structure, and avoid that the particles travel outside the field of view, the pro-

pellers were driven first forward and later backward when reaching the limit of the observation area. This change of direction was obtained by switching the x -component of the applied field, $H_x = -H_x$. Reversing the field does not disentangle the formed bound state since gravity and disorder break the symmetry under time inversion at low Reynolds number. From the particle positions, we determine the angle ϑ , and the velocities $\langle v_{cv} \rangle$, $\langle v_{rel} \rangle$ which now are averaged over all pairs of particles within the assembly. As shown in Fig.5(b), after a transient regime, all quantities stabilize to a stationary value where the relative speed between the composing particles approaches zero. The composite chain is rather stable, propelling as a compact rod with a center of velocity $\langle v_{cv} \rangle \sim 10 \mu\text{ms}^{-1}$. From Eq.1 it is also possible to calculate the net flow field velocity generated by the assembly, which is presented in the small inset in Fig.5(b) as a streamplot graph. The chain of propellers generates a net flux toward the direction of motion, perpendicular to the chain long axis and focused towards the center of the assembly. This flow field may be used to manipulate unbound non magnetic objects in a fluid, both pulling or pushing them by varying the propulsion direction of the chain through the sense of rotation of the actuating magnetic field. Plans to explore these exciting possibilities are under way.

In conclusion, we have investigated the long range hydrodynamic interactions between two model microswimmers composed by magnetically propelled anisotropic hematite particles. When HIs dominate over the dipolar one, we observe the emergence of cooperative states hydrodynamically bound, where the particles adjust their speed by slowing down or speeding up due to the generated flow field. Our findings may help understand similar cooperative mechanisms occurring in confined biological systems at low Reynolds number, and be a starting point towards the description of the dynamics in dense driven particle suspensions.

2 MATERIALS AND METHODS

Magnetic propellers and experimental set-up. Ellipsoidal hematite ($\gamma\text{-Fe}_2\text{O}_3$) particles are synthesized by following the technique developed by Sugimoto and coworkers (46). Specifically, we gradually add to an iron chloride hexahydrate solution (54.00g $\text{FeCl}_3 \cdot 6\text{H}_2\text{O}$ in 100ml of high deionized water) a sodium hydroxide solution (19.48g of NaOH in 90ml of Millipore water) and stir both solutions at 75°C . After 5min, we add to the stirring mixture 10ml of an aqueous solution containing 0.29g of potassium sulfate (K_2SO_4). The resulting brown mixture is then stirred for another 5min, hermetically sealed, and left aging in an oven at 100°C for 8 days.

The ellipsoidal-like particles are then recovered by diluting the suspension with high deionized water, letting the particles sediment and removing the resulting yellowish-brown supernatant, a procedure that is repeated several times. In order to avoid sticking of the particles to the glass substrate, the hematite ellipsoids are then functionalized with sodium dodecyl sulfate (SDS).

The measurement cell is placed in the center of two orthogonal pairs of coils arranged on the stage of an optical microscope and aligned along the x and z axis. To apply a rotating field in a plane, the two pair of coils are connected with a wave generator (TGA1244, TTI) feeding a power amplifier (AMP-1800, AKIYAMA or BOP 20-10M, Kepco) and two sinusoidal currents with 90degrees phase-shift are passed through the coils. The particle dynamics are recorded by using a CCD camera (Basler Scout scA640-74fc) working at 75 frame per second. The camera is mounted on top of a light microscope (Eclipse Ni, Nikon) equipped with different magnification objectives ($100\times$, $40\times$) and a $0.45\times$ TV lens adapter. The positions of the particles are obtained from the analysis of .AVI videos recorded via a commercial software (streampix, NORPIX).

Determination of the magnetic moments. We measure the distribution of magnetic mo-

ments by following the orientation of different hematite particles subjected to an external static magnetic field \mathbf{H} , as shown in the schematic in Fig.1(c). In first approximation, we assume that the shape of our hematite particle resembles that of an ellipsoid, and thus use the friction coefficient of ellipsoid in water to describe the particle dynamics. When reoriented by the external field, the magnetic torque acting on the ellipsoid, $\boldsymbol{\tau}_m = \mu_0 \mathbf{m} \times \mathbf{H}$, is balanced by the viscous torque arising from its rotation in the fluid, $\boldsymbol{\tau}_v = -\xi_r \dot{\boldsymbol{\theta}}$. Here $\mu_0 = 4\pi \cdot 10^{-7} \text{H m}^{-1}$ and ξ_r the rotational friction coefficient of the ellipsoid. By solving the torque balance equation, $\boldsymbol{\tau}_m + \boldsymbol{\tau}_v = 0$, and taking into account that the angle between the permanent moment and the ellipsoid long axis is $\pi/2$, we arrive at the equation:

$$\theta(t) = 2 \tan^{-1} \left[\tanh \left(\frac{t}{\tau_r} \right) \right]. \quad (2)$$

The rotational friction coefficient for a prolate ellipsoid rotating around its short axis can be written as $\xi_r = 8\pi\eta V_c f_r$, where $V_c = (4\pi ab^2)/3$ is the volume of the ellipsoid, and f_r is a small geometrical factor which depends on the lengths of the ellipsoid long and short axes.

References

1. R. Dreyfus, *et al.*, *Nature* **437**, 862 (2005).
2. P. Tierno, R. Golestanian, I. Pagonabarraga, F. Sagués, *Phys. Rev. Lett.* **101**, 218304 (2008).
3. A. Snezhko, M. Belkin, I. S. Aranson, W.-K. Kwok, *Phys. Rev. Lett.* **102**, 118103 (2009).
4. L. Zhang, *et al.*, *Nano Lett.* **9**, 3663 (2009).
5. A. Bricard, J.-B. Caussin, N. Desreumaux, O. Dauchot, D. Bartolo, *Nature* **503**, 95 (2013).
6. W. F. Paxton, *et al.*, *J. Am. Chem. Soc.* **126**, 13424 (2004).
7. J. R. Howse, *et al.*, *Phys. Rev. Lett.* **99**, 048102 (2007).

8. I. S. Aronson, *Phys. Usp* **56**, 79 (2013).
9. J. E. Martin, A. Snezhko, *Reports on Progress in Physics* **76**, 126601 (2013).
10. M. Reichert, H. Stark, *Phys. Rev. E* **69**, 031407 (2004).
11. S. Martin, M. Reichert, H. Stark, T. Gisler, *Phys. Rev. Lett.* **97**, 248301 (2006).
12. C. Lutz, M. Reichert, H. Stark, C. Bechinger, *EPL (Europhysics Letters)* **74**, 719 (2006).
13. A. Ziehl, J. Bammert, L. Holzer, C. Wagner, W. Zimmermann, *Phys. Rev. Lett.* **103**, 230602 (2009).
14. N. Bruot, J. Kotar, F. de Lillo, M. Cosentino Lagomarsino, P. Cicuti, *Phys. Rev. Lett.* **109**, 164103 (2012).
15. H. Nagar, Y. Roichman, *Phys. Rev. E* **90**, 042302 (2014).
16. W. E. Uspala, P. S. Doyle, *Soft Matter* **10**, 5177 (2014).
17. R. Di Leonardo, *et al.*, *Phys. Rev. Lett.* **109**, 034104 (2012).
18. N. Koumakis, R. Di Leonardo, *Phys. Rev. Lett.* **110**, 174103 (2013).
19. J. Kotar, *et al.*, *Phys. Rev. Lett.* **111**, 228103 (2013).
20. E. Lauga, T. R. Powers, *Rep. Prog. Phys.* **72**, 096601 (2009).
21. M. C. Marchetti, *et al.*, *Rev. Mod. Phys.* **85**, 1143 (2013).
22. I. H. Riedel, K. Kruse, J. Howard, *Science* **309**, 300 (2005).
23. A. Vilfan, F. Jülicher, *Phys. Rev. Lett.* **96**, 058102 (2006).
24. B. Guirao, J. F. Joanny, *Biophys. J* **92**, 1900 (2006).

25. K. Drescher, *et al.*, *Phys. Rev. Lett.* **102**, 168101 (2009).
26. E. Lauga, W. R. DiLuzio, G. M. Whitesides, H. A. Stone, *Biophys. J.* **90**, 400 (2005).
27. A. P. Berke, L. Turner, H. C. Berg, E. Lauga, *Phys. Rev. Lett.* **101**, 038102 (2008).
28. M. B. Wan, C. J. Olson Reichhardt, Z. Nussinov, C. Reichhardt, *Phys. Rev. Lett.* **101**, 018102 (2008).
29. R. Di Leonardo, D. Dell'Arciprete, L. Angelani, V. Iebba, *Phys. Rev. Lett.* **106**, 038101 (2011).
30. A. Pototsky, A. M. Hahn, H. Stark, *Phys. Rev. E* **87**, 042124 (2013).
31. R. Ledesma-Aguilar, J. M. Yeomans, *Phys. Rev. Lett.* **111**, 138101 (2013).
32. A. Goldman, R. Cox, H. Brenner, *Chem. Eng. Sci.* **22**, 637 (1967).
33. F. Martinez-Pedrero, H. Massana-Cid, P. Tierno, *Small* **13**, 1603449 (2017).
34. R. Adler, *Proc. IRE* **34**, 351 (1946).
35. J. R. Blake, A. T. Chwang, *J. Eng. Math.* **8**, 23 (1974).
36. F. Martinez-Pedrero, A. Ortiz-Ambriz, I. Pagonabarraga, P. Tierno, *Phys. Rev. Lett.* **115**, 138301 (2015).
37. F. Martinez-Pedrero, P. Tierno, *Phys. Rev. Applied* **3**, 051003 (2015).
38. P. Lenz, J.-F. m. c. Joanny, F. Jülicher, J. Prost, *Phys. Rev. Lett.* **91**, 108104 (2003).
39. M. Baron, J. Bławdziewicz, E. Wajnryb, *Phys. Rev. Lett.* **100**, 174502 (2008).
40. M. Leoni, T. B. Liverpool, *Europhys. Lett.* **92**, 64004 (2010).

41. I. O. Götze, G. Gompper, *Europhys. Lett.* **92**, 64003 (2010).
42. K. Yeo, E. Lushi, P. M. Vlahovska, *Phys. Rev. Lett.* **114**, 188301 (2015).
43. Y. Goto, H. Tanaka, *Nat. Comm.* **6**, 5994 (2015).
44. F. Guzman-Lastra, A. Keiser, H. Lowen, *Nat. Comm.* **7**, 13519 (2016).
45. M. Driscoll, *et al.*, *Nat. Phys.* **13**, 375 (2017).
46. T. Sugimoto, A. Muramatsu, *J. Colloid Interface Sci.* **184**, 626 (1996).

Acknowledgments

F.M.P. , A.O.A. and P.T. acknowledge support from the ERC starting Grant "DynaMO" (No. 335040). F.M.P. acknowledges support from the Ramon y Cajal program (RYC-2015-18495). E.N.A. and I.P. acknowledges support from MINECO (Spain), Project FIS2015-67837-P, DURSI Project 2014SGR-922, and Generalitat de Catalunya under Program "ICREA Acadèmia". P.T. acknowledges support from from MINECO (FIS2016-78507-C2) and DURSI (2014SGR878).

SUPPLEMENTARY MATERIALS

As supporting Information we provide one .pdf file with the derivation of the set of equations used to fit the experimental data in the main text.

Supporting Information Movies

With the article are 4 videoclips as support of Figs.1,3 and Fig.4.

- **MovieS1**(.WMV) This videoclip illustrates the dynamics of a pair of propellers driven by a rotating magnetic field with amplitude $H_0 = 1500 \text{ Am}^{-1}$ and frequency $\omega = 31.4 \text{ rad s}^{-1}$

(left side), and $\omega = 502.6\text{rad s}^{-1}$ (right side). The video corresponds to Fig.1(e) of the article.

- **MovieS2**(.WMV) The video illustrate the increasing velocity of a pair of propellers driven by a rotating magnetic field with amplitude $H_0 = 4400\text{A m}^{-1}$ and frequency $\omega = 502.6\text{rad s}^{-1}$. The video corresponds to the middle row of Fig.2(b) of the article.
- **MovieS3**(.WMV) Assembly and transport of a chain composed by 5 propellers subjected to a rotating magnetic field with amplitude $H_0 = 4400\text{A m}^{-1}$ and frequency $\omega = 502.6\text{rad s}^{-1}$. During the video one component of the rotating field is inverted ($H_x = -H_x$) each time the collection of particles reaches the edge of the observation area. The video corresponds to Fig.5(a) of the article.
- **MovieS4**(.WMV) The video shows the trajectory of the center of a pair of particles in an hydrodynamic bound state obtained from numerical simulation of the equation of motion of the pair. The video corresponds to Fig.3(a) in this Supporting Information.

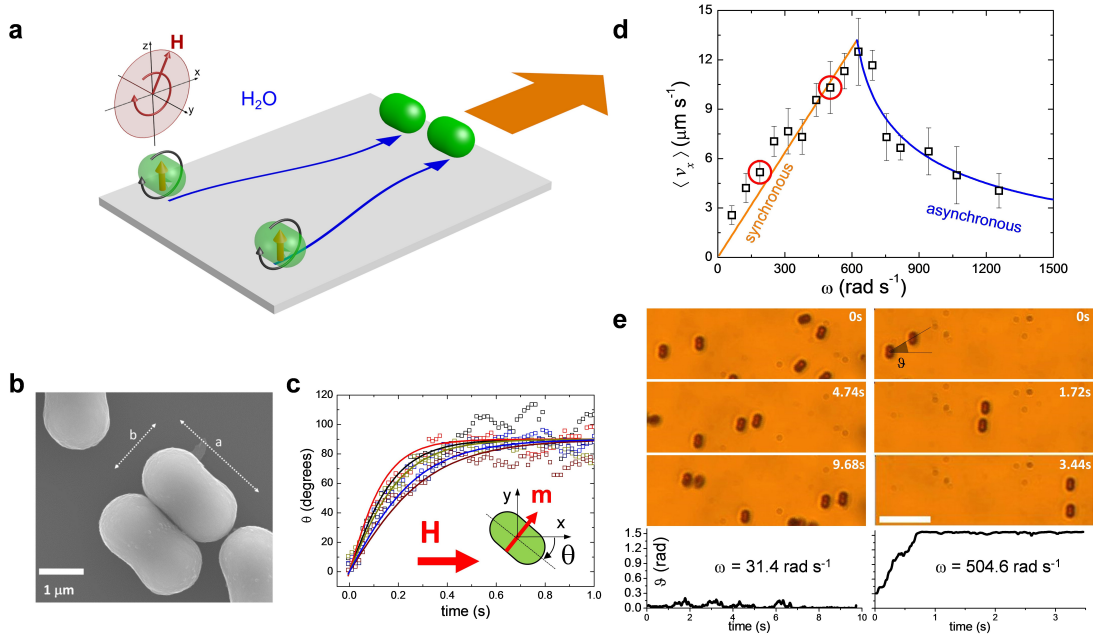


Figure 1: Propulsion of the hematite micropropellers. **(a)** Schematic showing two hematite particles subjected to a rotating magnetic field circularly polarized in the (x, z) plane. **(b)** SEM image of the hematite particles, being a and b the long and short axis, resp. **(c)** Orientational angle θ between the particle long axis and an applied field H . The particle moment is obtained by balancing the magnetic and viscous torque during re-orientation, see Method section. **(d)** Average speed $\langle v_x \rangle$ versus driving frequency ω of one micropropeller subjected to a rotating field with amplitude $H_0 = 4400 \text{ A m}^{-1}$. Orange (blue) fit denotes synchronous (asynchronous) regime. **(e)** Microscope images showing a pair of propelling particles at frequencies $\omega = 31.4 \text{ rad s}^{-1}$ (left) and $\omega = 502.7 \text{ rad s}^{-1}$ (right). Scale bar is $10 \mu\text{m}$, see MovieS1 in the Supplementary Information. Bottom panel shows the evolution with time of the relative positional angle θ .

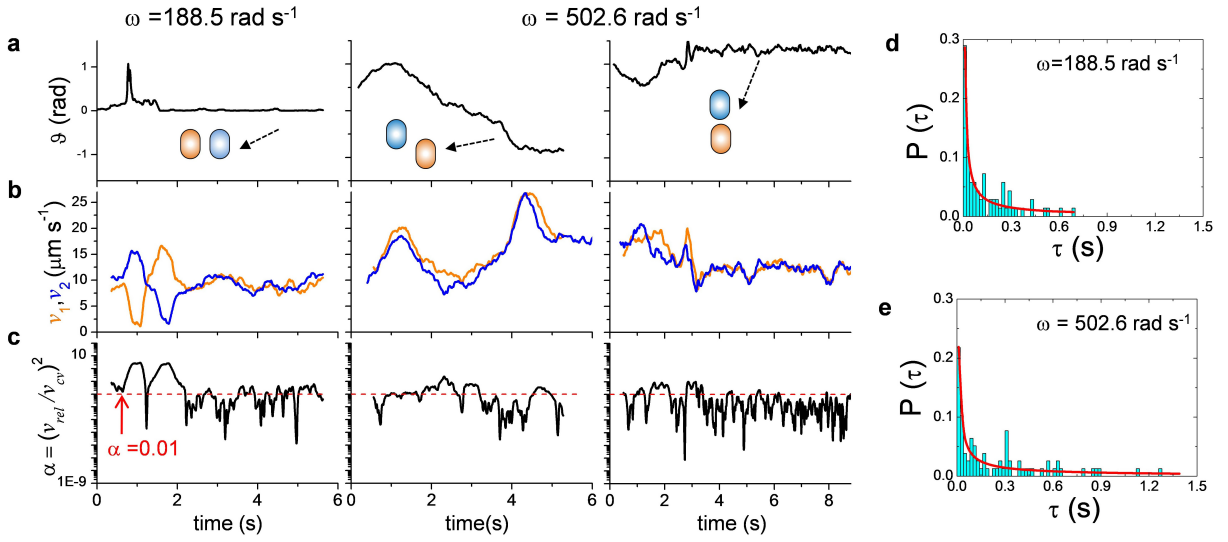


Figure 2: Observation of the bound states. **(a-c)** Sequence of graphs illustrating the evolution of the angle ϑ (a), particle velocities v_1, v_2 (b) and normalized relative velocity squared $\alpha = (v_{rel}/v_{cv})^2$ (c) versus time for a pair of propellers driven by a rotating field with amplitude $H_0 = 4400 \text{ A m}^{-1}$ and at two different frequencies. The first column refers to $\omega = 125.7 \text{ rad s}^{-1}$, second and third columns to $\omega = 502.6 \text{ rad s}^{-1}$. The increase in speed of the pair of propellers is shown in MovieS2 in the Supplementary Information. **(d,e)** Probabilities $P(\tau)$ of times τ where the pair of propellers have $\alpha < 0.01$ for frequencies $\omega = 125.7 \text{ rad s}^{-1}$ (d), and $\omega = 502.6 \text{ rad s}^{-1}$ (e). The continuous red line are fits to the data of an algebraic function as a guide to the eye.

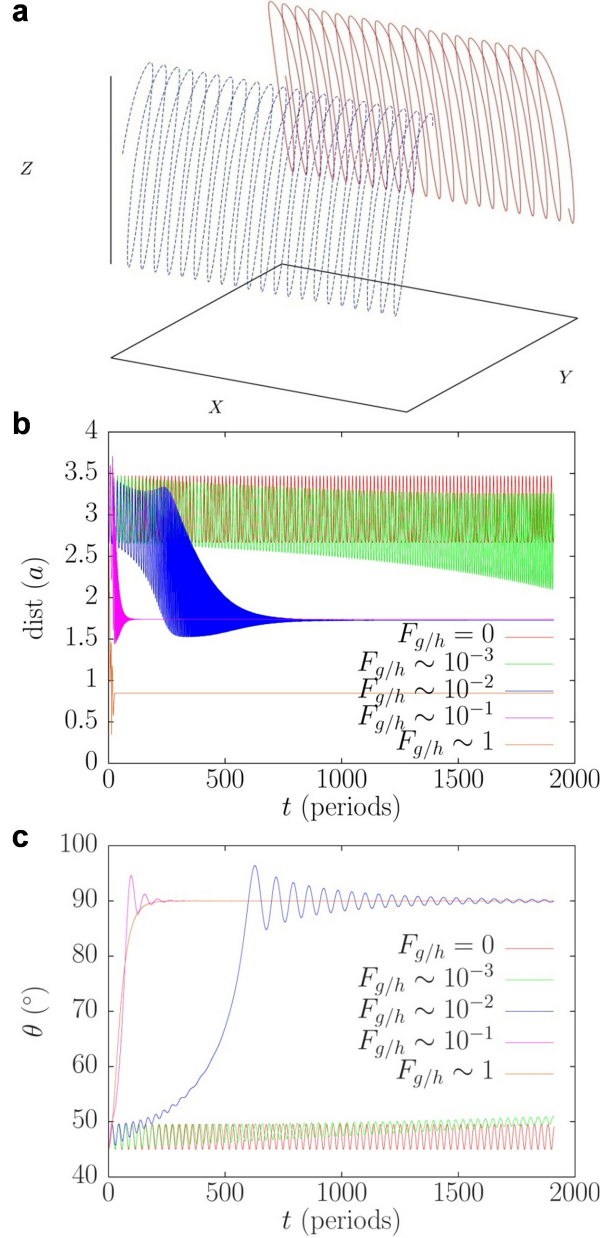


Figure 3: Hydrodynamic bound states. **(a)** Three dimensional trajectories of two particles (one in blue, the other in red) in a hydrodynamic bound state. The data are obtained from numerical simulations of the equations in the Supporting Information, with an initial angle $\vartheta = 45^\circ$ and at a distance of $d = 2.67a$, being a the particle radius, see MovieS4 in the Supplementary Information. **(b,c)** Distance (b) and angle (c) between the two particles measured in term of the particle radius a versus period of the driving field for different values of $F_{g/h}$, the latter denotes the ratio between the gravitational F_g and viscous F_h forces.

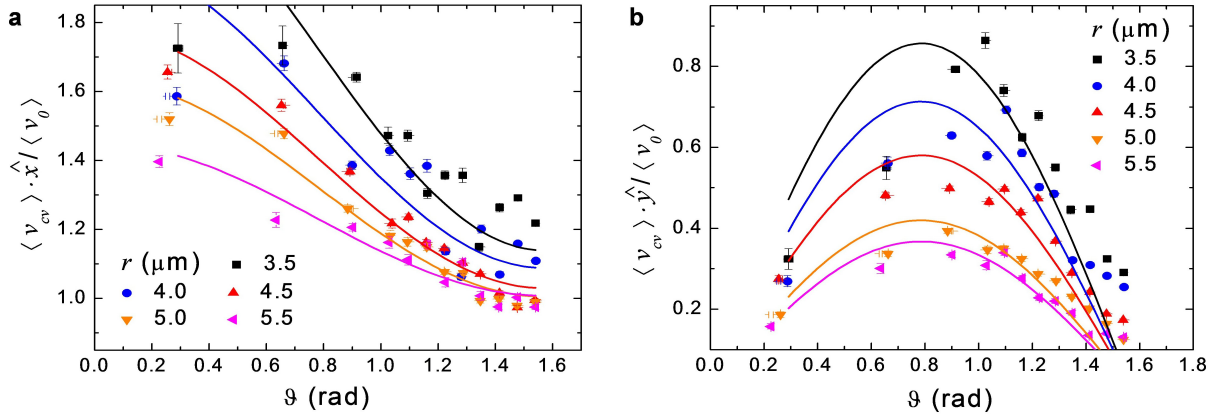


Figure 4: Average center of velocity of the pair. **(a,b)** Components of the velocity $\langle v_{cv} \rangle$ along the \hat{x} (a) and \hat{y} (b) directions, versus angle ϑ . The pair of propellers forming the bound states is driven by a rotating field with amplitude $H_0 = 4400 \text{Am}^{-1}$ and frequency $\omega = 502.6 \text{rad s}^{-1}$. $\langle v_0 \rangle = 10.3 \mu\text{m s}^{-1}$ denotes the speed of a single propeller driven by the same field, r is the center to center distance. Scattered symbols denote experimental data, continuous lines are fits following the model developed in the text.

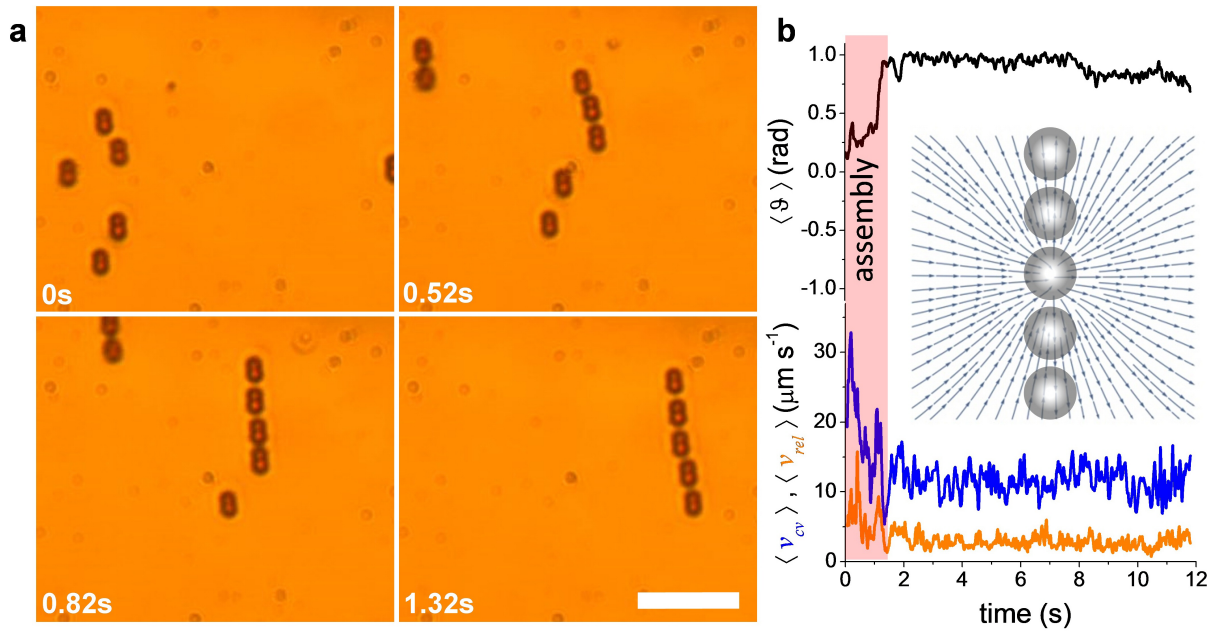


Figure 5: Self-assembly due to sole HI. **(a)** Sequence of images showing the formation of a chain of 5 propellers under a rotating field with amplitude $H_0 = 4400 \text{A m}^{-1}$ and frequency $\omega = 502.6 \text{rad s}^{-1}$. Scale bar is $10 \mu\text{m}$, the corresponding video, MovieS3, is in the Supplementary Information. **(b)** Evolution with time of the average positional angle ϑ (top), $\langle v_{cv} \rangle$ in blue and $\langle v_{rel} \rangle$ in orange (bottom). The shaded red region in the graph denotes the assembly stage. Inset illustrates the flow velocity u_x calculated at the same elevation of a chain composed of 5 propellers.